Analyst

Accepted Manuscript

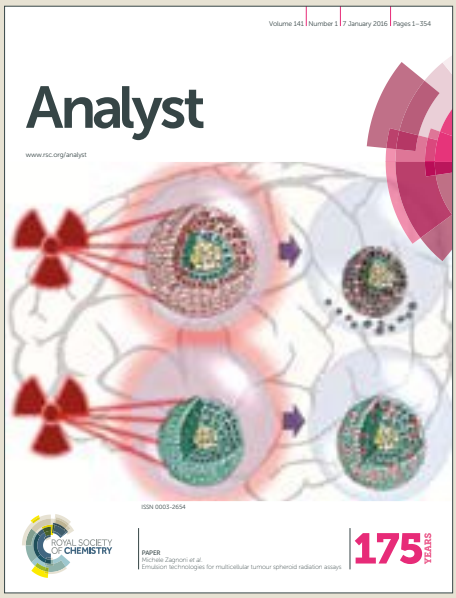

ROYAL SOCIETY OF CHEMISTRY

rsc.li/analyst

Journal Name

ROYAL SOCIETY OF CHEMISTRY View Article Online
DOI: 10.1039/C9AN00079H

ARTICLE

Real-time Monitoring of Peroxynitrite ($ONOO^-$) in the Rat Brain by Developing a Ratiometric Electrochemical Biosensor

Feiyue Liu, Hui Dong and Yang Tian*

Received 00th January 20xx,
Accepted 00th January 20xx

DOI: 10.1039/x0xx00000x

www.rsc.org/

As one of reactive oxygen species (ROS), peroxynitrite ($ONOO^-$) generated by nitric oxide (NO) and superoxide anion ($O_2^{\bullet-}$), plays important roles in the physiological and pathological processes in the brain. However, the lack of reliable and durable analytical methods in vivo is still the bottleneck to understand the signal pathway of $ONOO^-$ in the brain. In this work, a ratiometric electrochemical biosensor was developed for real-time monitoring and accurate quantification of $ONOO^-$ in the rat brain followed by cerebral ischemia. Firstly, a novel organic molecule, 4-(S-(6-mercaptohexyl) benzothioate-6-yl)-7-(diethylamino)-2-(4-(piperazinyl diferroformamide-1-yl)phenyl)chromenylium (HEMF) with specific recognition group toward $ONOO^-$ and electroactive group – ferrocence, was designed and synthesized for determination of $ONOO^-$ with high selectivity. The oxidation peak of ferrocence decreased with increasing concentration of $ONOO^-$ with a quick response within 15 s, because pyrylium group in HEMF molecule specifically reacted with $ONOO^-$, thus resulting in the drop of ferrocene group from HEMF molecule through ring-opening reaction. Meanwhile, 5′-MB-GGCGCGATTTT-SH-3′ (SH-DNA-MB) was optimized as an inner reference molecule, leading to the accurate quantification of $ONOO^-$ to avoid the environmental effects. The oxidation peak current ratio between ferrocence and MB demonstrated a good linearity with the concentration of $ONOO^-$ from 20.0 nM to 2.0 μM. The detection limit was achieved down to 12.1 ± 0.8 nM. The developed biosensor showed remarkable selectivity against potential interferences in the brain such as other ROS, metal ions, amino acids and bioactive species due to the specific reaction between pyrylium group and $ONOO^-$. As a result, the present ratiometric electrochemical biosensor with significant analytical performance including high temporal resolution, high selectivity and accuracy, combined with the unique characteristic of carbon fiber microelectrode (CFME) such as high spatial resolution and good biocompatibility, was successfully applied in real-time determination of $ONOO^-$ in the rat brain that followed by global cerebral ischemia.

Introduction

Peroxynitrite ($ONOO^-$), one kind of reactive oxygen species (ROS), is formed by nitric oxide (NO) and superoxide ($O_2^{\bullet-}$) with strong oxidizability[1] and unstability with a short half-life (0.9 s) at pH 7.4.[2] It can react with a large amount of biological species, such as proteins, lipids, nucleic acids and so on, eventually resulting in apoptosis even various clinical diseases, such as Alzheimer's diseases (AD), inflammatory, cancer, and angiocardiopathy.[3-6] On the other hand, the peroxynitrite-associated reactions that may modulate mitochondrial function[7] and maintaining sodium homeostasis both in the physiological and pathophysiological processes.[8] Nevertheless, the double-edged role of $ONOO^-$ is still controversial and the physiological and pathological process of $ONOO^-$ in brain have not been revealed. Thus, to develop an effective and reliable analytical method in vivo is the bottleneck to understand the physiological and pathological roles that $ONOO^-$ plays in the brain. To date, a great number of approaches have been established for determination of $ONOO^-$, including fluorescent probes, chemiluminescence, immunohistochemistry and so on.[9-12] Although the methods reported above may provide the real-time information of $ONOO^-$ in live cells and/or tissues, it is still hard to realize the real-time monitoring $ONOO^-$ in the brain with the whole network.

In vivo and real time analysis of chemical species directly in the brain is a vital pathway to investigate brain functions and brain diseases.[13-16] With the bursting study on the brain science, the important role of ROS in physiological and pathological processes of brain is attracting more and more attention.[17-19] Compared with other methods, electrochemical approaches demonstrate remarkable advantages for in vivo and real-time detection of biological species in the brain, such as high temporal resolution, high spatial resolution, and high sensitivity with real-time information.[20-28] In the earlier work of our group, we designed and constructed several electerochemical biosensors and fluorescent probes for selective and accurate recognition of biological species related to oxidative stress.[29-32] However, due to high reactivity and short lift-time of $ONOO^-$, it

Shanghai State Key Laboratory of Green Chemistry and Chemical Processes, Department of Chemistry, School of Chemistry and Molecular Engineering, East China Normal University, Dongchuan Road 500, Shanghai 200241, China. E-mail: ytian@chem.ecnu.edu.cn; Fax: +86-21-54341041.

Electronic Supplementary Information (ESI) available. See DOI: 10.1039/x0xx00000x

View Article Online
DOI: 10.1039/C9AN00070H

is still a great challenging work to create an electrochemical biosensor for real-time monitoring of $ONOO^-$ in the brain.

In this work, a selective and accurate electrochemical biosensor with high spatial and temporal resolution was developed for real-time monitoring of $ONOO^-$ levels in the different regions of rat brain followed by global cerebral ischemia as shown in Scheme 1. First of all, a new organic molecule, 4-(S-(6-mercaptohexyl) benzothioate-6-yl)-7-(diethylamino)-2-(4-(piperazinyl diferroformamide-1-yl) phenyl)chromenylium (HEMF) with specific recognition group toward $ONOO^-$ and electroactive group–ferrocence, was designed and synthesized for determination of $ONOO^-$ with high selectivity (Scheme 1A). The oxidation peak of ferrocence group in HEMF molecule was observed at 364 mV vs Ag/AgCl. This peak rapidly decreased with increasing concentration of $ONOO^-$, because pyrylium group in HEMF molecule specifically reacted with $ONOO^-$, resulting in the drop of ferrocene group from HEMF molecule through ring-opening reaction (Scheme 1B and Fig. S1). Secondly, 5′-MB-GGCGCGATTTT-SH-3′ (SH-DNA-MB) with oxidation peak at -88 mV vs Ag/AgCl was optimized as an inner reference element to improve accuracy. The current density ratio of these two peaks ascribed to oxidation of ferrocence and MB demonstrated a good linearity with the concentration of $ONOO^-$ ranging from 20.0 nM to 2.0 μM, with the limit of detection (3σ) down to 12.1 ± 0.8 nM (n = 6). The ratiometric biosensor showed high selectivity for determination of $ONOO^-$ against other ROS, metal ions, amino acids, and neurotransmitters, attributed to the specific reaction between designed molecule HEMF and $ONOO^-$. Finally,

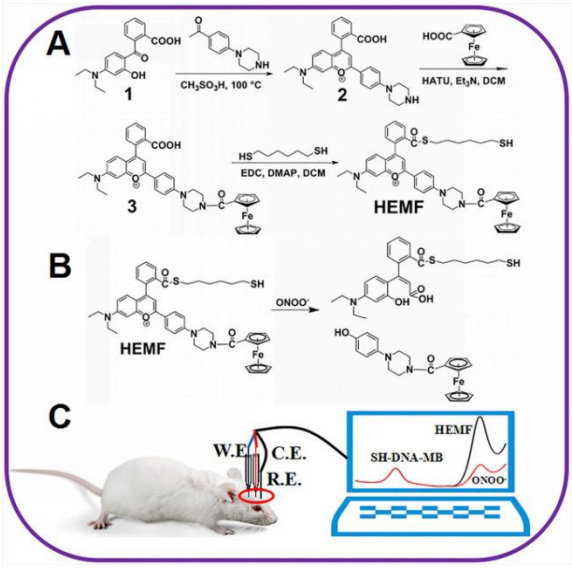

Scheme 1 The Developed Ratiometric Electrochemical Biosensor for Real-Time Monitoring of $ONOO^-$ Levels in the Rat Brain Followed by Global Cerebral Ischemia.

combined with the unique property of carbon fiber microelectrode (CFME) including high spatial resolution (10 μm) and good biocompatibility, the developed ratiometric electrochemical biosensor with high temporal resolution was successfully applied in detection of $ONOO^-$ in three regions of rat brain followed by cerebral ischemia (Scheme 1C).

Experimental section

Materials and chemicals

1,6-Hexanedithiol, chloroauric acid trihydrate ($HAuCl_4 \cdot 3H_2O$), dopamine (DA), L-cysteine (Cys), L-glutamine (Glu), glycine (Gly), L-arginine (Arg), L-histidine (His), L-methionine (Met), L-leucine (Leu), L-threonine (Thr), L-isoleucine (Iso), L-phenylalanine (Phe), L-serine (Ser), uric acid (UA), D(+)-glucose, 1-ethyl-3-(3-dimethyl-aminopropyl)carbodiimide (EDC), ascorbic acid (AA), 3-methoxytyramine hydrochloride (3-MT), 5-hydroxyindole-3-acetic acid (5-HIAA), DL-lactic acid, L-tyrosine, adenosine 5′-triphosphate disodium salt hydrate (ATP), tyramine, homovanillic acid (HVA) , methanesulfonic acid, 4′-piperazinoacetophenone, ferrocenecarboxylic were purchased from Sigma-Aldrich (America). 4-DimethylaMinopyridine (DMAP), sodium hypochlorite (NaClO), 30% hydrogen peroxide (H_2O_2), 2-(4-diethylamino-2-hydroxybenzoyl)benzoic acid, and $NaNO_2$ were purchased from Aladdin Chemistry Co. Ltd. (Shanghai, China). 5′-MB-GGCGCGATTTT-SH-3′ (SH-DNA-MB) was obtained from TaKaRa Biotechnology Co. Ltd. (Dalian, China). Triethylamine, NaOH, HCl, KH_2PO_4, KO_2, $K_2HPO_4 \cdot 3H_2O$, NaCl, KCl, $CaCl_2$, $NaNO_3$, $MgCl_2 \cdot 6H_2O$, $ZnCl_2$, $FeCl_2 \cdot 4H_2O$, $FeCl_3 \cdot 6H_2O$, H_2SO_4, $CuCl_2 \cdot 2H_2O$, $NaHCO_3$, Na_2SO_4, CH_3OH, and dimethyl sulfoxide (DMSO) were obtained from Sinopharm Chemical Reagent Co. Ltd (Shanghai, China). Artificial cerebrospinal fluid (aCSF) was prepared by mixing KCl (2.4 mM), NaCl (126 mM), KH_2PO_4 (0.5 mM), $NaHCO_3$ (27.5 mM), $CaCl_2$ (1.1 mM), $MgCl_2$ (0.85 mM), and Na_2SO_4 (0.5 mM) into Milli-Q water.

The preparation of ROS

The preparation of $ONOO^-$ solution was according to previous literature report.[33] Briefly, hydrochloric acid (0.6 M, 10 mL) was added to the mixture solution of hydrogen peroxide (0.7 M, 10 mL) and sodium nitrite (0.6 M, 10 mL), and then sodium hydroxide (1.5 M, 10 mL) was added within 1-2 s. Excess hydrogen peroxide in the solution was removed by a column of manganese dioxide. And then the resulting solution was split into small aliquots and stored at -20 °C. The absorption peak of $ONOO^-$ at 302 nm was used to determine the concentration of $ONOO^-$. The standard extinction coefficient of $ONOO^-$ in 0.1 M NaOH solution at 302 nm is 1,670 M^{-1} cm^{-1}. In selectivity experiments,[31,34,35] singlet oxygen ($^1O_2$) was generated by the reaction of H_2O_2 (20 μM) and NaClO (20 μM). Hydroxyl radical (• OH) was generated by the reaction of Fe^{2+} and H_2O_2 (Fe^{2+}/H_2O_2 = 1:6), the concentration of •OH was considered to be equal to the Fe^{2+} concentration. Superoxide anion ($O_2^{\bullet-}$) was derived from dissolved KO_2 (20 μM) in the DMSO solution, the concentration of $O_2^{\bullet-}$ was determined by measuring the reduction of ferricytochrome c spectrophotometrically and the extinction coefficient of ferrocytochrome c at 550 nm is 21.1 mM^{-1} cm^{-1}. NaClO solution was diluted appropriately in 0.1 M

View Article Online
DOI: 10.1039/C9AN00078H

NaOH soulution. The concentration of ClO^- was determined based on the molar extinction coefficient at 292 nm (350 M^{-1} cm^{-1}). Nitrate anion (NO_3^-), nitrite anion (NO_2^-) was provided by $NaNO_3$ (20 μ M) and $NaNO_2$ (20 μ M), respectively. All chemicals were analytical grade and commercially available. Milli-Q water (18.2 MΩ cm^{-1}) was applied for preparation of all aqueous solutions.

Preparation and modification of electrodes

The carbon fiber (~ 10 μm diameter) was purchased from Tokai Carbon Co. (Tokai, Japan). The preparation of carbon fiber microelectrode (CFME) was described as follows. Firstly, a carbon fiber was attached to a clean copper wire by using silver conducting paste. Secondly, a dried glass capillary (1.5 mm diameter, 100 mm length) was pulled on a microelectrode puller and divided into two parts of the same length. After that, the copper wire with carbon fiber was carefully threaded into the pulled capillary. Finally, the capillary was sealed with epoxy resin using a syringe and then dried in an oven at 120 ℃ for 4 h. Before modification, the length of carbon fiber on CFME was cut to 500 μm under a microscope, and the prepared CFME was sequentially sonicated in acetone, 3 M HNO_3, 1.0 M KOH, and distilled water each for 3 min. Then, under a potential of -0.2 V vs Ag/AgCl in 0.1 M $HClO_4$ containing 10 mM $HAuCl_4$ solution for 120 s, the nanostructured Au leaves were electrodeposited on the pretreated CFME. The Au nanoleave-electrodeposited electrode was denoted as CFME/Au. The CFME/Au electrode was immerged in methanol solution of SH-DNA-MB and HEMF saturated by N_2 gas for 6 h. Such an electrode was denoted CFME/Au/MB+HEMF. The CFME modified with only SH-DNA-MB by the same way was denoted as CFME/Au/MB.

Instruments and measurements

The scanning electron microscopy (SEM) image was taken by Hitachi S-4800 field emission scanning electron microscope. Infrared spectrum was carried out by Fourier Transform-Infrared Spectrometer (FT-IR, Nicolet iS10, Thermo Electron, America). X-ray photoelectron spectroscopy (XPS, AXIS Ultra DLD, Japan) equipped with an Al Kα (1486.6 eV photons) was used to characterize the electrode modification processes. NMR spectroscopy was taken using Bruker AV-400 spectrometer. X-ray diffraction (XRD) was obtained by a Shimadzu XRD-6000. Electrochemical experiment was performed on an electrochemical work station (CHI 660D, Chenhua in Shanghai, China) with a standard three-electrode system consisting of a reference electrode (Ag/AgCl) and a platinum (Pt) wire as counter electrode. The absorbance of cytotoxicity was conducted by a Varioskan LUX multimode microplate reader (Thermo Fisher Scientific). The apoptosis assay was taken by FACSCalibur flow cytometry (Becton Dickinson and Co.). All measurements were carried out at an ambient temperature.

In vivo detection

All procedures involving animals were conducted with an approval of the Animal Ethics Committee in East China Normal University, China. The experimental methods and surgeries were performed as previously report.[36-38] Briefly, the adult male rats and ischemia model rats (250-300 g, Shanghai SLAC Laboratory Animal Co. Ltd. Shanghai, China) were anesthetized by using chloral hydrate with an initial dose of 300 mg/kg (i.p.). Then, the rats were fixed on a stereotaxic frame (Beijing Tide-Gene Biotechnology Development Center). After that, CFME/Au/MB+HEMF electrode was implanted in the different regions in rat brain of the dorsal hippocampus (AP = 5.0 mm, L = 5.0 mm from bregma, V = 2.5 mm from the surface of the skull), the left striatum (AP = 0 mm, L = 2.5 mm anterior to the bregma, and V = 7.0 mm from the surface of skull), the cortex (AP = 0.2 mm, L = 5.6 mm from the bregma, V = 3.0 mm from the surface of skull), according to standard stereotaxic procedures. Reference and counter electrodes were implanted into the dura of the rat brain through a 2 mm plastic cannula. In order to reduce injury of the rat, the CFME/Au/MB+HEMF electrode should be implanted within 30 min, slowly and carefully. Throughout the operation, supplements of chloral hydrate (100 mg/kg) were given as required, and the body temperature of the rats were maintained at 37 ° C with a thermic blanket (Beijing Tide-Gene Biotechnology Development Centre).

Cytotoxicity and apoptosis assays

For cytotoxicity assay, different concentrations of HEMF, SH-DNA-MB and ferrocene which may fall into the rat brain after reacted with $ONOO^-$ were added into pre-incubated neurons in 96-well plates and cultured for 24 and 48 h, respectively. Then, 40 μL of MTT solution was added to each well in the dark. After reaction for 4 h, the mixed solution was removed and 80 μL of DMSO was added to each well. After shaking for 5 min, the absorbance was measured at 490 nm. The cell viability values were determined according to the following formulas: cell viability (%) = absorbance of experimental group/absorbance of blank control group × 100%.

For apoptosis assay, different concentrations of HEMF, SH-DNA-MB and ferrocene which may fall into the rat brain after reacted with $ONOO^-$ were cultured with neurons for 24 h. After removal of the culture medium, the neurons were collected with the help of EDTA-free trypsin. After the neurons were washed by PBS, the neurons were re-suspended in 300 μL of binding buffer and stained with 5 μL FITC-Annexin V and 5 μL propidium iodide solution for 30 min in dark. Apoptosis assay was analyzed by flow cytometer at an excitation wavelength of 480 nm.

Results and discussion

Characterization of the CFME and modified electrodes

As a starting point of this work, a novel organic molecule HEMF including pyrylium and ferrocene groups, was designed and synthesized, as illustrated in Scheme 1A, in which pyrylium group showed specific recognition toward $ONOO^-$ through ring-opening reaction while the electroactive ferrocene group provided the eletrochemical signal. The products of each step were characterized by ^1H NMR, ^{13}C NMR, MS, and FTIR spectroscopy (Fig. S2-S5). Meanwhile, for amplifying the signals,

View Article Online
DOI: 10.1039/C8AN00070H

the gold nanostructures were electrodeposited on the CFME surface, which was denoted as CFME/Au electrode.

As shown in Fig. 1, the diameter of CFME is ~10 μm (Fig. 1A), and the nanoleave-like gold structures were clearly observed onto CFME electrode surface (Fig. 1B). From the enlarged SEM image, the length of Au nanoleaves was estimated to ~2-8 μm (Fig. 1C). As demonstrated in the XRD pattern (Fig. 1D), three typical peaks 38.1°, 44.3°, 65.6° corresponding to (111), (200), (220) diffraction peaks were clearly obtained, indicating that the observed nanoleave-like structures were composed of poly-crystal gold. The current density of HEMF oxidation peak obtained at CFME/Au electrode was ~5.6-fold compared with that obtained at bare gold electrode, possibly due to the amplified property of gold nanomaterials (Fig. S6). On the other hand, SH-DNA-MB was synthesized and optimized as a reference element, providing a built-in correction to avoid the environmental effects especially in the complicated brain system. The simultaneous modification of SH-DNA-MB and HEMF on the CFME/Au electrode was characterized by X-ray spectroscopy (XPS, Fig. S7). After Au nanoleaves were electrodeposited on CFME, obvious peaks located at 84.0 eV and 87.7 eV for Au $4f_{7/2}$ and Au $4f_{5/2}$ (curve b, c and d, Fig. S7A) were obtained. The P 2p peak at 133.7 eV (curve c and d, Fig. S7B), and the S 2p peak at 162.0 eV (curve c and d, Fig. S7C) indicated the successful modification of SH-DNA-MB and HEMF on CFME/Au electrode through Au-S bond. Meanwhile,

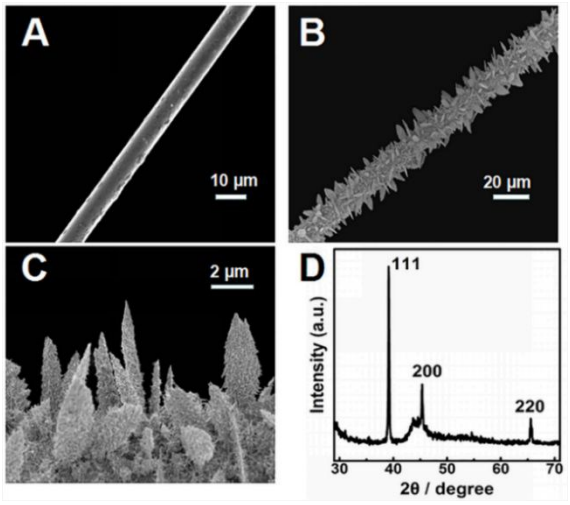

Fig. 1 SEM images of CFME (A), CFME electrodeposited with Au nanoleaves (CFME/Au) (B), the enlarged Au nanoleaves (C), and XRD pattern of Au nanoleaves (D).

the presence of Fe $2p_{3/2}$ (708.3 eV) and Fe $2p_{1/2}$ (720.2 eV) in Fig. S7D (curves d) also demonstrated the successful modification of HEMF, while no obvious peaks were observed at the controlled electrodes (curves a, b and c, Fig. S7D).

Electrochemical response of the CFME/Au/MB + HEMF electrode

Next, differential pulse voltammetry (DPV) was used to evaluate analytical performance of the developed biosensor, because of its high sensitivity. As demonstrated in Fig. 2, only an anodic peak at -88 mV versus Ag/AgCl for CFME/Au/MB was clearly observed (curve c), which was attributed to oxidation of MB in SH-DNA-MB, while no obvious peaks were obtained for CFME and CFME/Au (curves a and b). Moreover, a new anodic peak located at 364 mV vs Ag/AgCl was observed for CFME/Au/MB+HEMF electrode (curves d). This new anodic peak should be ascribed to the oxidation of ferrocence group of HEMF modified on electrode surface. The oxidation peak quickly went down with the addition of $ONOO^-$ because of the specific reaction between pyrylium group in HEMF and $ONOO^-$, resulting in drop of ferrocene group through ring-opening reaction. The reaction product was evaluated by Liquid chromatography-mass spectrometry (Fig. S8) and the mechanism of HEMF and $ONOO^-$ was illustrated in Scheme 1B. Furthermore, the response time of CFME/Au/MB+HEMF electrode toward different concentrations of $ONOO^-$ was tested. As shown in Fig. S9, $j_p/j_{p(R)}$ value remained stable after 15 s at the constant concentration (1.0 μM, 1.5 μM and 2.0 μM) of $ONOO^-$, namely the oxidation current of ferrocence was unchanged after pyrylium group in HEMF was reacted with $ONOO^-$ within 15 s. The sensor response should be stable within 15 s, namely the electrochemical signal maintained unchanged within just 15 s.

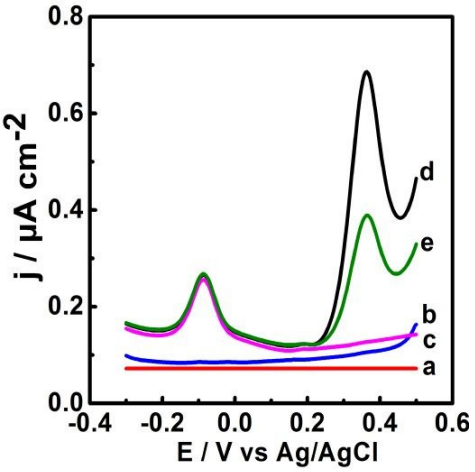

Fig.2 DPVs obtained at (a) CFME, (b) CFME/Au, (c) CFME/Au/MB, (d) CFME/Au/MB+HEMF, and (e) CFME/Au/MB+HEMF electrodes in aCSF (pH 7.4) with addition of 1.0 μM $ONOO^-$.

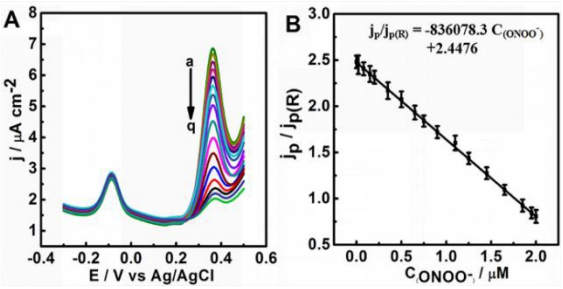

Fig. 3 (A) DPVs obtained at CFME/Au/MB+HEMF electrode in aCSF (pH 7.4) with addition of different concentrations of $ONOO^-$ (From a to q: 0, 0.02, 0.08, 0.15, 0.20, 0.35, 0.50, 0.65, 0.75, 0.90, 1.10, 1.25, 1.45, 1.65, 1.85, 1.95, 2.00 μM). (B) The linear relationship of the peak current density ratio ($j_p/j_{p(R)}$) obtained at 364 mV and -88 mV vs Ag/AgCl with different concentrations of $ONOO^-$.

Moreover, as demonstrated in Fig. 3A, the oxidation peak at 364 mV (j_p) decreased with increasing concentrations of $ONOO^-$, while that of MB at -88 mV ($j_{p(R)}$) was almost constant, resulting in the ratiometric determination of $ONOO^-$. The current intensity ratio ($j_p/j_{p(R)}$) between these two peaks showed a good linearity with the concentration of $ONOO^-$ ranging from 20.0 nM to 2.0 μM. The limit of detection (3σ) was estimated down to 12.1 nM ± 0.8 (n = 6). Moreover, the same CFME/Au/MB+HEMF electrode toward addition of $ONOO^-$ from lower to higher concentrations, and then down to lower concentration was also tested. As shown in Fig. S10, the Δj (the peak current difference of ferrocence at 364 mV) versus Δ $C_{(ONOO^-)}$ (the concentration difference of $ONOO^-$) of $ONOO^-$ from low to high (50 nM to 400 nM) and from high to low (400 nM to 50 nM) also demonstrated a good linearity, which proved the accuracy of the principle of the development electrochemical sensor. Furthermore, the stability of CFME/Au/MB+HEMF electrode was also tested. The value of $j_p/j_{p(R)}$ exhibited negligible changes (< 3.6%) after the constant scanning in PBS (pH 7.4) for 500 cycles (Fig. S11). In addition, the $j_p/j_{p(R)}$ value of CFME/Au/MB+HEMF decreases by only 4.0% for storing in refrigerator for 6 days in darkness, indicating this electrode had good stability (Fig. S12).

Selectivity tests

More importantly, it is still a great challenge for in vivo analysis with high selectivity in the complicated rat brain system. In this work, selectivity test was evaluated in aCSF solution (pH 7.4) induced by potential interferences, including ROS (O_2, $^1O_2$, ClO^-, NO, H_2O_2, •OH, $O_2•^-$, NO_2^-, NO_3^-), metal ions (K^+, Na^+, Ca^{2+}, Mg^{2+}, Zn^{2+}, Cu^{2+}, Cu^+, Fe^{3+}, Fe^{2+}), amino acids (Met, Iso, Phe, Ser, Cys, Glu, Gly, His, Leu, Arg, Thr) and other bioactive species (DA, UA, AA, Glucose, 3-MT, 5-HIAA, HVA, Tyramine, DL-lactic acid) that coexist in the brain system against $ONOO^-$. On the one hand, little interferences (< 7.4%) were observed with addition of ROS, metal ions, amino acid, and other potential interferences (Fig. 4A-D). On the other hand, for the competition test, when all the above compounds were added

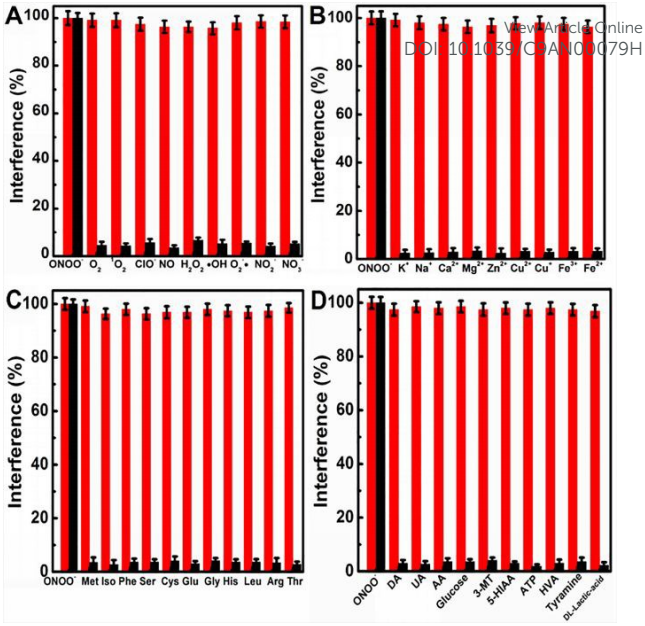

Fig. 4 (A) Selectivity (black bars) and competition (red bars) tests of ROS against $ONOO^-$. (a) O_2, (b) $^1O_2$, (c) ClO^-, (d) NO, (e) H_2O_2, (f) •OH, (g) $O_2•^-$, (h) NO_2^-, (i) NO_3^- (200 μM for a, 20 μM for b to i). Competition experiments were carried out by the subsequent addition of 1.0 μM $ONOO^-$ to the solutions containing other ROS. (B) Selectivity (black bars) and competition (red bars) tests of metal ions against $ONOO^-$. (a) K^+, (b) Na^+, (c) Ca^{2+}, (d) Mg^{2+}, (e) Zn^{2+}, (f) Cu^{2+}, (g) Cu^+, (h) Fe^{3+}, (i) Fe^{2+} (100 mM for a and b, 1 mM for c, 10 μM for d to i). Competition experiments were carried out by the subsequent addition of 1.0 μM $ONOO^-$ to the solutions containing metal ions. (C) Selectivity (black bars) and competition (red bars) tests of amino acids against $ONOO^-$: (a) Met, (b) Iso, (c) Phe, (d) Ser, (e) Cys, (f) Gly, (g) His, (h) Leu, (i) Arg, (j) Thr (10 μM for a to j). Competition experiments were carried out by the subsequent addition of 1.0 μM $ONOO^-$ to the solutions containing amino acids. (D) Selectivity (black bars) and competition (red bars) tests of biological species against $ONOO^-$. (a) DA, (b) UA, (c) AA, (d) glucose, (e) 3-MT, (f) 5-HIAA, (g) HVA, (h) Tyramine, (i) DL-lactic acid (1 mM for d, 10 μM for others). Competition experiments were carried out by the subsequent addition of 1.0 μM $ONOO^-$ to the solutions containing biological species.

followed by addition of $ONOO^-$, negligible changes (< 2.8%) were obtained. All the results indicate that the developed ratiometric biosensor showed high selectivity for $ONOO^-$ detection against ROS, metal ions, amino acid, and other biological species, due to the specific recognition of HEMF toward $ONOO^-$. In addition, no obvious changes (6.2%) of the $j_p/j_{p(R)}$ value was obtained when pH ranged from 6.6 to 8.2 at the CFME/Au/MB+HEMF electrode (Fig. S13). Meanwhile, $j_p/j_{p(R)}$ value maintained almost unchanged (< 2.4%) for six different electrodes, revealing CFME/Au/MB+HEMF electrode demonstrated good reproducibility (Fig. S14).

View Article Online
DOI: 10.1039/C9AN00079H

Determination of ONOO⁻ in vivo

As demonstrated above, the developed biosensor for determination of ONOO⁻ showed good selectivity, improved accuracy, high temporal resolution, as well as long-term stability. The remarkable analytical performance, together with the unique property of CFME such as high spatial resolution and good biocompatibility, the present electrochemical biosensor was applied to evaluate the levels of ONOO⁻ in the rat brain. Before in vivo determination, the standard MTT colorimetric assay and the flow cytometry experiments of the neurons treated with HEMF, SH-DNA-MB and ferrocene which may fall into the rat brain after reacted with ONOO⁻, at high dosages (1.0 μ M) were carried out to evaluate the cytotoxicity and biocompatibility (Fig. S15 and S16). The cellular viabilities of neurons incubated with HEMF, SH-DNA-MB and ferrocene molecules at 1.0 μ M concentration which is about 10^4-fold higher than those used in measurements in rat brain for 24 h and 48 h showed greater than 91% (Fig. S15), demonstrating that HEMF, SH-DNA-MB and ferrocene molecules are low toxic for neurons. As shown in Fig. S16, negligible differences were found between control neurons and the neurons treated with HEMF, SH-DNA-MB and ferrocene, revealing good biocompatibility of these molecules. And as demonstrated in Fig. 5A, the post-calibration curve was plotted after detection in the rat brain. The slope of post-calibration only deceased by 2.8%, compared with that of calibration curve plotted in aCSF, as shown in Fig. 3B and Fig. 5A. Fig. 5B shows DPV responses obtained at CFME/Au/MB+HEMF electrode in the hippocampus of (a) normal rat brain and (b) rat brain followed by cerebral ischemia for 30 min. It was found that the value of $j_p/j_{p(R)}$ gradually decreased in the hippocampus of rat brain followed

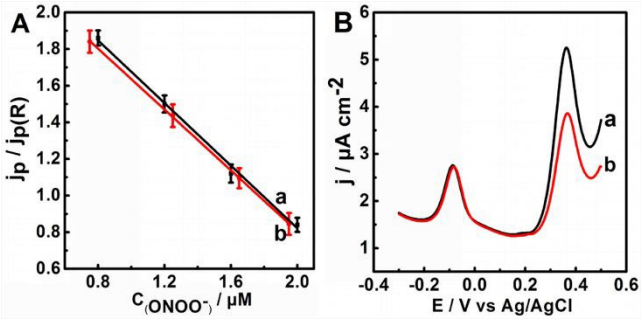

Fig. 5 (A) The $j_p/j_{p(R)}$ value of post-calibration (a) and calibration plot (b) with different concentrations of ONOO⁻ from 0.8 μM to 2.0 μM. (B) DPVs obtained at CFME/Au/MB+HEMF electrodes for ONOO⁻ determination in hippocampus of (a) normal rat brain and (b) rat brain followed by cerebral ischemia for 30 min.

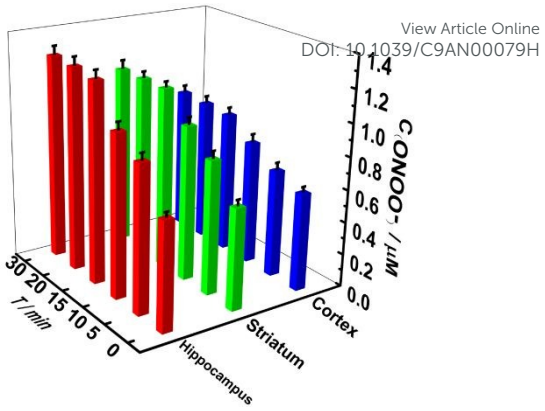

Fig. 6 Levels of ONOO⁻ determined in hippocampus, striatum, and cortex regions of rat brain followed by global cerebral ischemia with different time.

by cerebral ischemia for 5 to 30 min, and kept almost constant after 30 min. According to the post-calibration (Fig. 5B), the level of ONOO⁻ in hippocampus of normal rat brain followed by ischemia for 30 min was estimated to 1.17 ± 0.02 μM, which is significantly greater than that obtained in the normal rat brain, 572 ± 9 nM. Furthermore, the levels of ONOO⁻ in other regions such as cortex and striatum of rat brain followed by global cerebral ischemia with different time were also investigated and summarized in Fig. 6. Because ONOO⁻ plays important roles in the physiological and pathological processes related to brain diseases, for example, ischemia.[3,4] In the one hand, the hippocampus, cortex and striatum in rat brain are the typical regions closely related with oxidation stress processes, particular for ischemia process.[32,38,39] On the other hand, according to previous reports,[40-42] the ONOO⁻ and the ONOO⁻-associated reactions have close relationships with the three regions of hippocampus, cortex and striatum when rat brain followed by cerebral ischemia. Therefore, three regions of hippocampus, cortex and striatum in rat brain were chosen as typical brain regions to detect the variation of ONOO⁻ in brain regions with ischemia.

The results indicated that the levels of ONOO⁻ increased by 80.2 ± 9.3% (n = 3) in striatum, 53.5 ± 11.1% (n = 3) in cortex and 103.9 ± 7.4% (n = 3) in hippocampus within 30 min, compared with those obtained in the normal brains (n means different rats). The observed data demonstrated that $O_2^{\bullet -}$ and NO may give a burst after cerebral ischemia and thus to form ONOO⁻.[40,43]

Conclusions

In summary, we developed a selective and accurate electrochemical biosensor for real-time determination and quantification of ONOO⁻ in the rat brain, in which HEMF was designed and synthesized as the specific recognition molecule for ONOO⁻ and SH-DNA-MB was optimized as an inner reference element. The developed electrochemical biosensor showed

View Article Online
DOI: 10.1039/C9AN00079H

remarkable selectivity for $ONOO^-$ determination against ROS, metal ions, amino acids and other bioactive species, due to the specific reaction between pyrylium group in HEMF and $ONOO^-$, resulting in drop of ferrocene group through ring-opening reaction. The present electrochemical biosensor with high temporal and spatial resolution, as well as long-term stability and good reproducibility was applied to evaluate the levels of $ONOO^-$ in hippocampus, striatum, and cortex of rat brain followed by cerebral ischemia. This work has established an effective and reliable approach for real-time quantification of $ONOO^-$ in normal rat brain and rat brain followed by ischemia, which may help us and other scientists to understand the roles that $ONOO^-$ plays in the brain. More importantly, the investigation has also provided a methodology for designing and constructing ratiometric electrochemical biosensors for detection of other ROS, metal ions and bioactive species in the brain, which may play important roles in physiological and pathological process in brain.

Conflicts of interest

There are no conflicts to declare.

Acknowledgements

This work was financially supported by NSFC (21635003) and National Nature Science Fund for Distinguished Young Scholars (21325521). The Program of Shanghai Subject Chief Scientist (15XD1501600) is gratefully acknowledged. This work also was supported by Innovation Program of Shanghai Municipal Education Commission (201701070005E00020).

Compliance with Ethical Standards:

This study was funded by National Nature Science Fund (grant number 21635003, 21325521); The Program of Shanghai Subject Chief Scientist (15XD1501600); Innovation Program of Shanghai Municipal Education Commission (201701070005E00020).

Ethical Approval: All animal experiments in this study were performed in strict accordance with an approval of the Animal Ethics Committee in East China Normal University with the following reference number (m20170402), China.

Notes and references

1 G. Ferrer-Sueta, N. Campolo, M. Trujillo, S. Bartesaghi, S. Carballal, N. Romero, B. Alvare and R. Radi, *Chem. Rev.,* 2018, **118**, 1338.
2 J. S. Beckman, T. W. Beckman, J. Chen, P. A. Marshall and B. A. Freeman, *Proc. Natl. Acad. Sci. USA.,* 1990, **87**, 1620.
3 F. Torreilles, T. Salman-Tabcheh, M. Guérin and J. Torreilles, *Brain Res. Rev.,* 1999, **30**, 153.
4 C. Szabó, H. Ischiropoulos and R. Radi, *Nat. Rev. Drug Discov.,* 2007, **6**, 662.
5 C. Szabó and K. Módis, *Shock*., 2010, **34**, 4.
6 N. Loukili, N. Rosenblatt-Velin, J. Li, S. Clerc, P. Pacher, F. Feihl, B. Waeber and L. Liaudet, *Cardiovasc. Res.,* 2011, **89**, 586.
7 R. Radi, A. Cassina, R. Hodara, C. Quijano and L. Castro, *Free Radic. Biol. Med.,* 2002, **33**, 1451.
8 A. K. Maiti, M. T. Islam, R. Satou and D. S. A. Majid, *Physiol. Rep.,* 2016, **4**, 1.
9 D. Cheng, Y. Pan, L. Wang, Z. Zeng, L. Yuan, X. Zhang and Y. Chang, *J. Am. Chem. Soc.,* 2017, **139**, 285.
10 Z. Wang, X. Teng and C. Lu, *Anal. Chem.,* 2015, **87**, 3412.
11 Z. Song, D. Mao, H. P. S. Simon, T. K. K. Ryan, W. Y. L. Jacky, D. Kong, D. Ding and B. Tang, *Adv. Mater.,* 2016, **28**, 7249.
12 L. Viera, Y. Z. Ye, A. G. Estevez and J. S. Beckman, *Methods Enzymol.,* 1999, **301**, 373.
13 J. M. Goldberg and S. J. L. Lippard, *Acc. Chem. Res.,* 2017, **50**, 577.
14 F. Wu, P. Yu and L. Mao, *Chem. Soc. Rev.,* 2017, **46**, 2692.
15 Y. Luo, L. Zhang, W. Liu, Y. Yu and Y. Tian, *Angew. Chem. Int. Ed.,* 2015, **127**, 14259.
16 J. Zhang, A. Jaquins-Gerstl, K. M. Nesbitt, S. C. Rutan, A. C. Michael and S. G. Weber, *Anal. Chem*., 2013, **85**, 9889.
17 P. Kopelman, Y. E. L. Kooa, M. Philbert, B. A. Moffat, G. R. Reddy, P. McConville, D. E. Hall, T. L. Chenevert, M. S. Bhojani, S. M. Buck, A. Rehemtulla and B. D. J. Ross, *Magn. Magn. Mater.,* 2005, **293**, 404.
18 M. Yamato, T. Egashira and H. Utsumi, *Free Radic. Biol. Med.,* 2003, **35**, 1619.
19 Z. Yu, A. J. Bruce-Keller, Y. Goodman and M. P. Mattson, *J. Neurosci. Res.,* 1998, **53**, 613.
20 H. Lee, T. Choi, Y. Lee, H. Cho, G. Roozbeh, L. Wang, H. Choi, T. Chung, N. Lu, H. Taeghwan, S. Choi and D. Kim, *Nat. Nanotechnol.,* 2016, **11**, 566.
21 X. Chai, X. Zhou, A. Zhu, L. Zhang, Y. Qin, G. Shi and Y. Tian, *Angew. Chem. Int. Ed.,* 2013, **52**, 8129.
22 L. Zhang, Y. Han, F. Zhao, G. Shi and Y. Tian, *Anal. Chem.,* 2015, **87**, 2931.
23 T. Xiao, F. Wu, J. Hao, M. Zhang, P. Yu and L. Mao, *Anal. Chem.,* 2017, **89**, 300.
24 Y. Wang, Y. Liu, J. Xu, Y. Qin and W. Huang, *Anal. Chem.,* 2018, **90**, 5977.
25 X. Hu, Y. Liu, W. Wang, H. Zhang, Y. Qin, S. Guo, X. Zhang, L. Fu and W. Huang, *Anal. Chem.,* 2018, **90**, 1136.
26 S. Wang, X. Liu and M. Zhang, *Anal. Chem.,* 2017, **89**, 5382.
27 R. Li, X. Liu, W. Qiu and M. Zhang, *Anal. Chem.,* 2016, **88**, 7769.
28 H. Gu, E. L. Varner, S. R. Groskreutz, A. C. Michael and S. G. Weber, *Anal. Chem.,* 2015, **87**, 6088.
29 W. Wang, L. Zhang, L. Li and Y. Tian, *Anal. Chem.,* 2016, **88**, 9518.
30 Q. Xu, W. Liu, L. Li, F. Zhou, J. Zhou and Y. Tian, *Chem. Commun.,* 2017, **53**, 1880.
31 H. Huang, F. Dong and Y. Tian, *Anal. Chem.,* 2016, **88**, 12294.
32 L. Liu, L. Zhang, Z. Dai and Y. Tian, *Analyst*, 2017, **142**, 1452.
33 W. R. Janice, H. H.Hansel and L. J. William, *J. Am. Chem. Soc.,* 1974, **96**, 1248.
34 H. Dong, L. Zhang, W. Liu and Y. Tian, *ACS Chem. Neurosci.,* 2017, **8**, 339.
35 J. Zhou, L. Zhang and Y. Tian, *Anal. Chem.,* 2016, **88**, 2113.
36 W. Liu, H. Dong, L. Zhang and Y. Tian, *Angew. Chem. Int. Ed.,* 2017, **56**, 16328.
37 F. Zhao, L. Zhang, A. Zhu, G. Shi and Y. Tian, *Chem. Commun.,* 2016, **52**, 3717.
38 L. Liu, F. Zhao, W. Liu, T. Zhu, J. Z. H. Zhang, C. Chen, Z. Dai, H. Peng, J. Huang, Q. Hu, W. Bu and Y. Tian, *Angew. Chem. Int. Ed.,* 2017, **129**, 10607.
39 S. Li and Y. Tian, *Electroanalysis,* 2018, **30**, 1047.
40 P. H. J. Chan, *Cereb. Blood Flow Metab.,* 2001, **21**, 2.
41 A. Y. Estevez, S. Pritchard, K. Harper, J. W. Aston, A. Lynch, J. J. Lucky, J. S. Ludington, P. Chatani, W. P. Mosenthal, J. C.

View Article Online
DOI: 10.1039/C9AN00079H

Leiter, S. Andreescu and J. S. Erlichman, *Free Radic. Biol. Med.,* 2011, **51**, 1155.
42 M. Thiyagarajan, C. L. Kaul and S. S. Sharma, *Brit. J. Pharmacol.,* 2004, **142,** 899.
43 M. Thiyagarajan and S. S. Sharma, *Life Sci.,* 2004, **74**, 969.

View Article Online
DOI: 10.1039/C9AN00079H

TOC